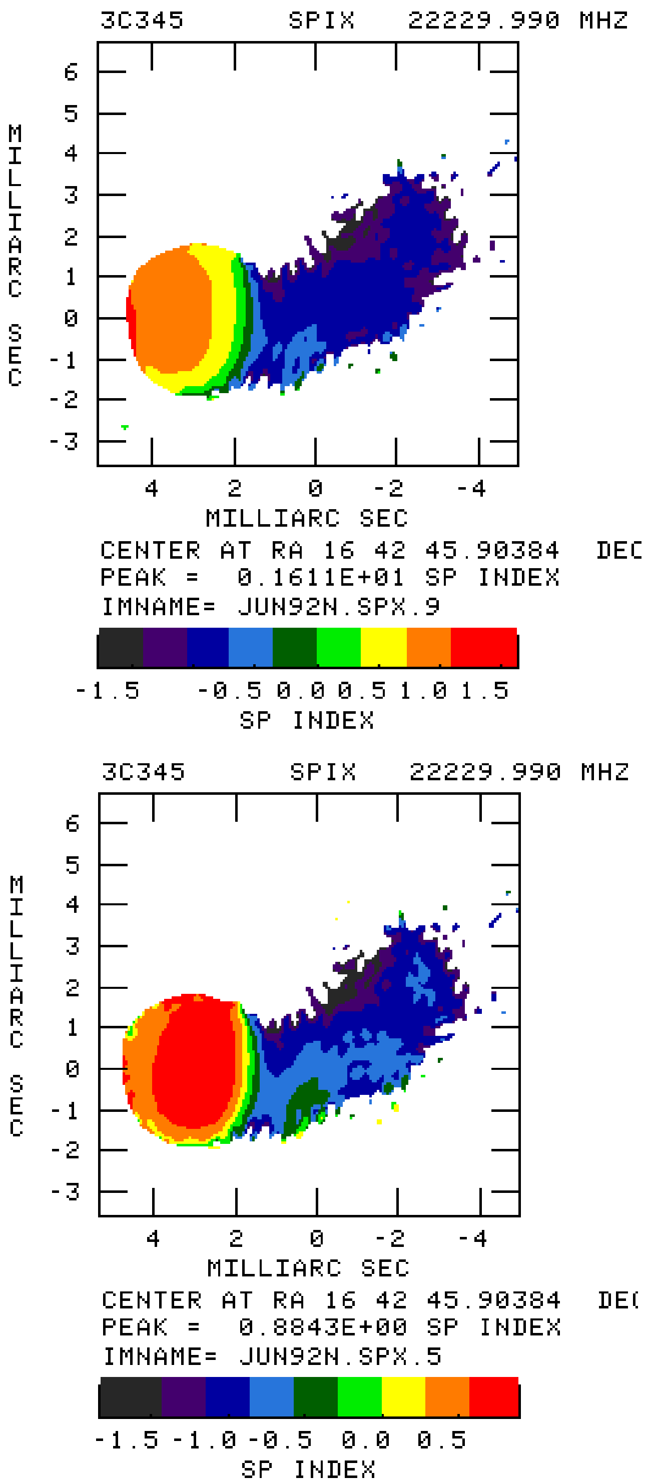

Figure 4.9: Spectral index maps of 3C345 made between 5 and 22.3 GHz (epoch: 1992.45). Top panel shows the original map, bottom panel shows the map corrected for the frequency dependent shift of the core position.

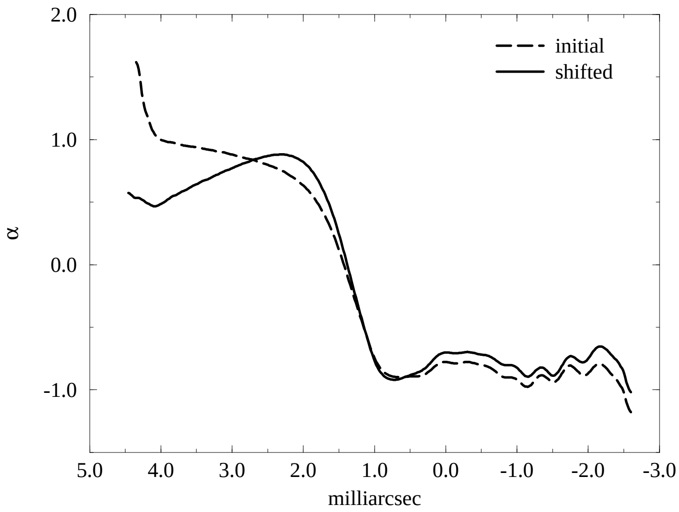

Figure 4.10: Spectral index profiles for the epoch 1992.45. The profiles are taken along the relative declination $\delta = 0$ mas. Dashed line gives the profile for the unshifted map, solid line presents the profile for the shifted map. The location of the core corresponds to 3 mas offset.

indicating possible effect of the core shift.

In the corrected map (bottom panel of Figure 4.11), the spectral index of the core and blended components is distributed very homogeneously, with mean value $\alpha \approx 0.2$. The latter is consistent with our estimates made from the Gaussian models, as well as with general predictions about spectral index of an undisturbed core (Blandford & Königl 1979).

Similarly to the spectral index map from the epoch 1992.45, the spectral index distribution of the extended emission is dominated by the flux variations at 22.3 GHz.

4.3 Synchrotron spectrum of the bright components

In spectral index maps, the only available kind of information is the spectral slope between the two frequencies. While sufficient for many purposes, this information can be misleading in the situation when the frequency of spectral maximum lies between the frequencies of spectral index mapping. In the ranges of frequencies between 1.6 and 22 GHz frequently used for VLBI observations, such a situation can be quite common. Using observations at three or more frequencies, it is possible to estimate the shape of synchrotron spectrum, and derive the turnover frequency (frequency of spectral maximum). Information about the turnover frequency can help in avoiding the confusion which is likely to occur in spectral index maps. The turnover frequency

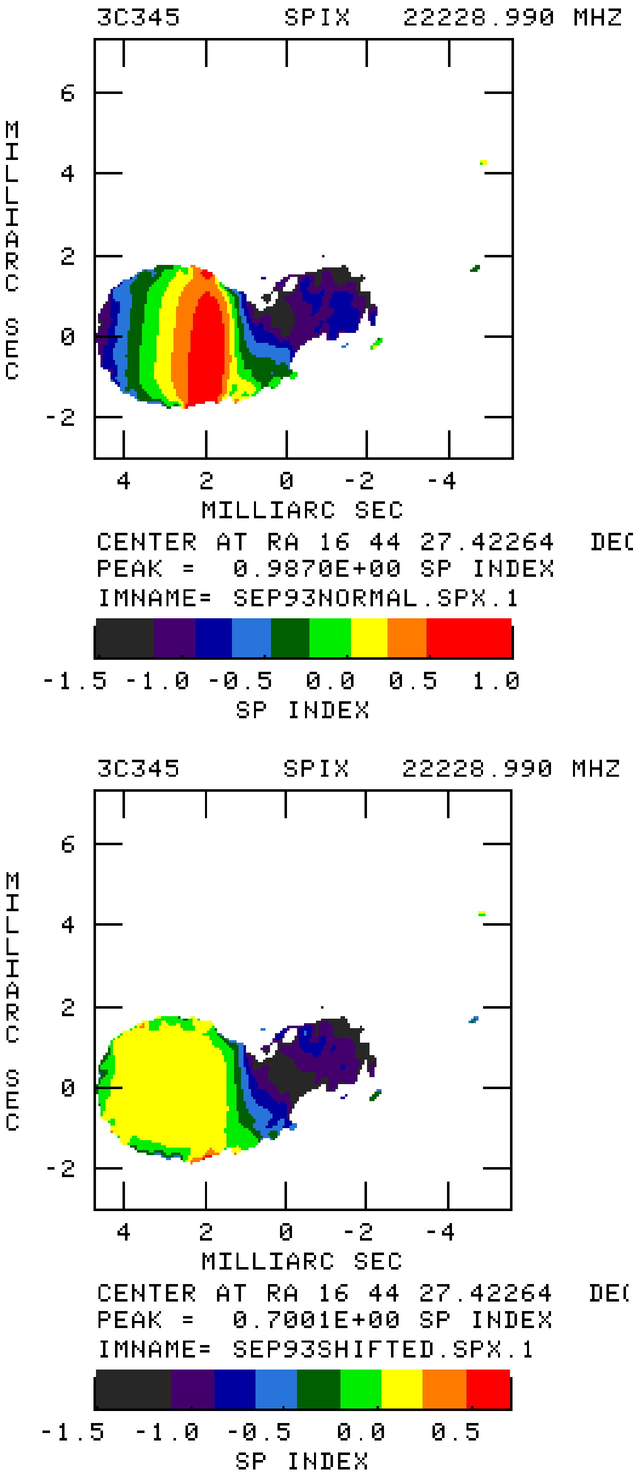

Figure 4.11: Spectral index maps of 3C345 made between 5 and 22.3 GHz (epoch: 1993.70). Top panel shows the original map, bottom panel shows the map corrected for the frequency dependent shift of the core position.

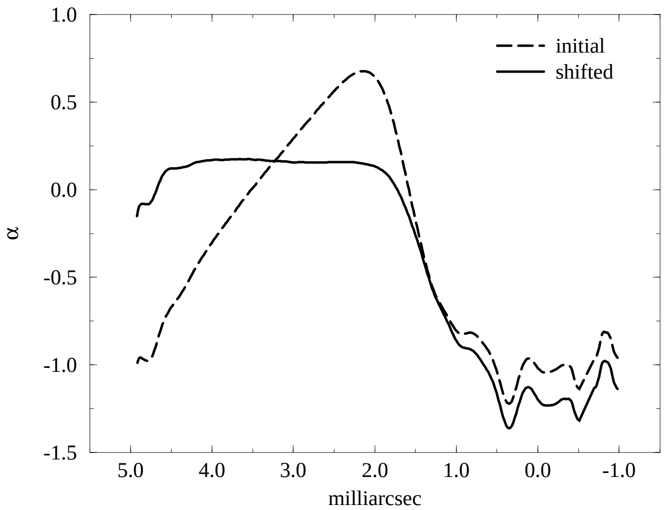

Figure 4.12: Spectral index profiles for the epoch 1993.70. The profiles are taken along the relative declination $\delta = 0$ mas. Dashed line gives the profile for the unshifted map, solid line presents the profile for the shifted map. The location of the core corresponds to 3 mas offset.

is sensitive to changes of physical conditions in the jet such as velocity, particle density, and magnetic field strength. This makes it an excellent tool for probing the physics of the jet in more detail than is allowed by analysis of flux and spectral index properties of the jet.

4.3.1 Synchrotron spectrum

For extensive and in–depth consideration of synchrotron emission and its properties, we refer to the works by Ginzburg and Syrovatskii (1969), Pacholczyk (1970), and Ternov and Mikhailin (1986). In our calculations, we use a simplistic approach, and consider synchrotron emission from a plasma with isotropic pitch angle distribution and power law energy distribution

$$n(\gamma)d\gamma = n_{\gamma_0}\gamma^{-s}d\gamma, \tag{4.4}$$

for electron Lorentz factors $\gamma_L < \gamma < \gamma_H$. In this case, it would suffice to describe the emission within the range of frequencies $\nu_L \ll \nu \ll \nu_H$, where $\nu_{L,H}$ are the *low–frequency* and *high–frequency* cutoffs given by:

$$\nu_{L,H} \approx \gamma_{L,H}^2 \frac{\Omega_e}{\pi}, \tag{4.5}$$

with Ω_e being the electron gyro–frequency. Then, for a plasma with electron self–absorption, the spectral distribution of emission is:

$$I_\nu = \frac{j_\nu}{\kappa_\nu}\left(1 - e^{-\kappa_\nu \tau}\right) \tag{4.6}$$

(Pacholczyk 1970), where j_ν is the synchrotron emissivity, κ_ν is the self–absorption coefficient and τ is the line–of–sight depth through the source. It is shown (Pacholczyk 1970) that Equation 4.6 can be rewritten as:

$$I_\nu = I_0 \left(\frac{\nu_1}{\nu_0}\right)^{-2} \left(\frac{\nu}{\nu_1}\right)^{2.5} \left\{1 - \exp\left[-\left(\frac{\nu_1}{\nu}\right)^{2.5-\alpha}\right]\right\}, \tag{4.7}$$

where ν_1 is the frequency at which $\tau = 1$; ν_0 is the frequency at which τ is negligible; I_0 is the surface brightness measured at the frequency ν_0 and α is the spectral index defined as $S \propto \nu^\alpha$. It is clear from equation 4.7 that at frequencies $\nu \ll \nu_1$: $I_\nu \propto (\nu/\nu_1)^{2.5}$; and at frequencies $\nu \gg \nu_1$: $I_\nu \propto 1 - \exp[-(\nu_1/\nu)^{2.5-\alpha}]$. These two spectral forms describe the *optically thick* and *optically thin* parts of the spectrum, respectively. We will use the description given by (4.7) in our subsequent calculations.

4.3.2 Correction for calibration errors

The flux data are taken from the model fits to the VLBI structure of the source (see Tables 2.4–2.16). Standard deviations for the model parameters are determined through the χ^2 estimations available in the "ERRFIT" routine of the Caltech VLBI software (for more detail on model fitting, see Chapters 2,3)

To correct the initial data for overall calibration errors (the overall antenna gain deviations, which are essentially unknown), a procedure of determining the *mean frame* and a model deviation from the mean frame is implemented.

The flux errors of the VLBI data were normalized using the assumption that radio variability of an AGN is restricted mostly to the compact structures around the galactic nucleus, and is not significant in extended structures over the time scales comparable with total duration of the monitoring programs. In this case, the offset between VLBI flux S_v and total flux S_t, ideally, must remain constant. For each VLBI observation, this offset and its standard deviation are

$$S_{off} = S_t - S_v, \quad \sigma^2_{off} = \sigma^2_t + \sigma^2_i \tag{4.8}$$

An estimate of the flux expected to come from extended structures can be made for each frequency of observations either by selecting the epoch known for the best amplitude calibration, or by finding the weighted average of S_{off} over all observations $t_{1,\dots,n}$ made at given frequency

$$S_{lobe} = \sigma^2_{lobe} \sum_{i=1}^{n} \left(\frac{S_{off}(t_i)}{\sigma_{off}(t_i)}\right), \quad \sigma^2_{lobe} = \left[\sum_{i=1}^{n}\left(\frac{1}{\sigma_{off}(t_i)}\right)\right]^{-1} \tag{4.9}$$

We use the best calibration rather than the mean value, to estimate S_{lobe}. This provides us with a self–consistent flux scale sufficient to reflect relative changes of the VLBI flux with respect to the chosen epoch of the best amplitude calibration.

With S_{lobe} determined through one of the abovementioned steps, the flux scale correction $\wp$ for each individual observation is

$$\wp = \frac{S_v}{S_t - S_{lobe}}, \quad \sigma_\wp^2 = \left(\frac{\sigma_\wp^2 + \sigma_{lobe}^2}{(S_t - S_{lobe})^2} + \frac{\sigma_v^2}{S_v^2} \right) \wp^2 \tag{4.10}$$

so that for a component with measured flux S_m, the normalized flux S_c will be

$$S_c = S_m \wp, \quad \sigma_c^2 = S_c^2 \left(\frac{\sigma_m^2}{S_m^2} + \frac{\sigma_\wp^2}{\wp^2} \right) \tag{4.11}$$

4.3.3 Spectral cutoffs

The frequency range covered by VLBI observations is very narrow (roughly, from 1 to 100 GHz, with most of the observations done between 5 and 22 GHz). Therefore, some additional constraints must be used to provide consistency of fits to the data. For synchrotron emission, the most plausible choice of such parameters is to use the low–frequency and high–frequency spectral cutoffs.

Because the transition between high–frequency ($\nu > \nu_1$) and low–frequency ($\nu < \nu_1$) spectral regimes determined by equation 4.7 is very sharp, the spectrum is determined by the synchrotron self–absorption at frequencies $\nu \ll \nu_1$, and by the electron energy distribution at $\nu \gg \nu_1$. Estimates of the turnover frequency and energy spectral index in the jet of 3C345 based on the calculations made for C4 by Rabaça and Zensus (1994) are:

$$\nu_1 \approx 10 GHz; \quad s \approx 2.8$$

Using these values, we estimate the low–frequency and high–frequency cutoffs in the spectrum: $\nu_l \sim 1\,\mathrm{MHz}$, $\nu_h \sim 1000\,\mathrm{GHz}$. We use these values for the spectral fitting. However, the cutoffs cannot be well defined, and are possibly subject to change during the evolution of the jet emission. To account for this effect, we allow 15% variations of the cutoff frequencies so as to achieve the best fit (*loose cutoff method*). The loose cutoff method will be described in Section 4.3.5.

4.3.4 Monte Carlo modeling

In order to calculate the spectral parameters of emission from a jet component, we combine the component fluxes measured at frequencies $\nu_1, ..., \nu_N$, and add the cutoff information. The resulting *spectral dataset* S_s, σ_s^2 is represented by

$$\{S_s\} = \{S(\nu_l), S(\nu_1), ..., S(\nu_N), S(\nu_h)\}, \quad \{\sigma_s^2\} = \{\sigma_S^2(\nu_l), \sigma_S^2(\nu_1), ..., \sigma_S^2(\nu_N), \sigma_S^2(\nu_h)\} \tag{4.12}$$

where $S(\nu_l) = S(\nu_h) = 1\,\mathrm{mJy}$ is the cutoff flux level.